A One-Structure-Based Hybridized Nanogenerator for Scavenging Mechanical and Thermal Energies by Triboelectric–Piezoelectric–Pyroelectric Effects

Shuhua Wang, Zhong Lin Wang, and Ya Yang**

Converting mechanical and thermal energies from the environment into electric energy has attracted increasing attentions in the past decade not only for dealing with the global energy crises, but also for achieving self-powered electronics.[1–6] However, since the mechanical and thermal energies are not always available at the same time, it is expected to develop a hybridized nanogenerator to simultaneously/individually scavenge the two kinds of energy. Previous investigations are mainly focused on how to integrate the different nanogenerators in series or in parallel.[7–11] In fact, some nanomaterials have multiphysical properties, such as poly(vinylidene fluoride) (PVDF) with piezoelectric, pyroelectric, and triboelectric properties,[12–15] which may be utilized to fabricate a hybridized nanogenerator with a one-material structure but exhibiting different functions for simultaneously scavenging different kinds of energy. Due to that the different nanogenerators have the same materials and current/voltage circuits, the coupling effect may appear in the hybridized device. It would be highly desirable to develop this kind of hybridized nanogenerator not only to miniaturize the device but also to couple the advantages of nanogenerators based on different mechanisms for realizing high output performance. Although the individual piezoelectric, triboelectric, or pyroelectric nanogenerators have been extensively investigated,[16–21] there has been no report on a single device that can simultaneously scavenge mechanical and thermal energy by utilizing the piezoelectric, triboelectric, and pyroelectric effects.

In this work, we fabricated a highly transparent, flexible, and hybridized nanogenerator based on a PVDF nanowires–poly(dimethylsiloxane) (PDMS) composite film as the triboelectric layer, a polarized PVDF film as both the piezoelectric and pyroelectric layers, and indium tin oxide (ITO) electrodes. The transmittance of the PVDF nanowires–PDMS composite film as the triboelectric material layer exhibited a controlled modulation effect with the changing ratio of up to 95% by utilizing the stretched strain and heated temperature. The hybridized nanogenerator with a one-device structure and the same electrodes can simultaneously deliver output current/voltage signals of triboelectric nanogenerators (TENGs), piezoelectric nanogenerators (PiENGs), and pyroelectric nanogenerators (PyENGs). As compared with the TENG–PiENG or the PyENG, the hybridized nanogenerator has a much better charging performance for a 10 μF capacitor.

Figure 1a illustrates a scanning electron microscopy (SEM) image of the random-oriented PVDF nanowires through the electro-spinning method, where the diameters of the PVDF nanowires are ranged from 200 to 500 nm. As displayed in Figure 1b, the cross-section SEM image of the PVDF nanowires–PDMS composite film indicates that the PVDF nanowires were fully dispersed in the PDMS film and the thickness of the PVDF nanowires–PDMS composite film is about 40 μm. To understand the crystal structure of the composite film, X-ray diffraction (XRD) spectra of PVDF nanowires, PDMS, and PVDF nanowires–PDMS composite film were measured, as displayed in Figure 1c. The crystallization of PVDF nanowires is mainly β-phase ($2\theta = 20.7°$) and α-phase ($2\theta = 17.9°$), while the peak at $2\theta = 12°$ is due to the PDMS film.[22,23] In this study, the PVDF nanowires–PDMS composite film was utilized as the transparent triboelectric materials for the TENG devices.

It is very interesting to observe that the stretched strain can induce a change in the transmittance of the PVDF nanowires–PDMS composite film. As displayed in Figure 1d, the transmittance of the composite film was found to increase with increasing the wavelengths ranging from 250 to 900 nm. The transparency of the composite film was found to decrease drastically after the first stretching treatment. To clearly observe the change in transmittance of the composite film, the composite film was placed on a paper with printed text. As visualized in Figure 1e, the composite film is transparent in the initial state. After the composite film was stretched, the transmittance of the composite film was decreased, resulting in that the printed text cannot be seen on the paper, as displayed in Figure 1f. Moreover, after the stretched composite film was heated at 250 °C for 1 min, the transmittance of the composite film can be recovered to the initial state, as illustrated in Figure 1g. The changing process of the transmittance due to the stretched strain and heated temperature can also be seen in Movie S1 (see the Supporting Information). To investigate the repeatability of the change in transmittance for the PVDF nanowires–PDMS composite film due to the stretched strain and heated temperature, the transmittance of the composite film

S. Wang, Prof. Z. L. Wang, Prof. Y. Yang
Beijing Institute of Nanoenergy and Nanosystems
Chinese Academy of Sciences
Beijing 100083, China
E-mail: yayang@binn.cas.cn
Prof. Z. L. Wang
School of Materials Science and Engineering
Georgia Institute of Technology
Atlanta, GA 30332-0245, USA
E-mail: zlwang@gatech.edu

DOI: 10.1002/adma.201505684

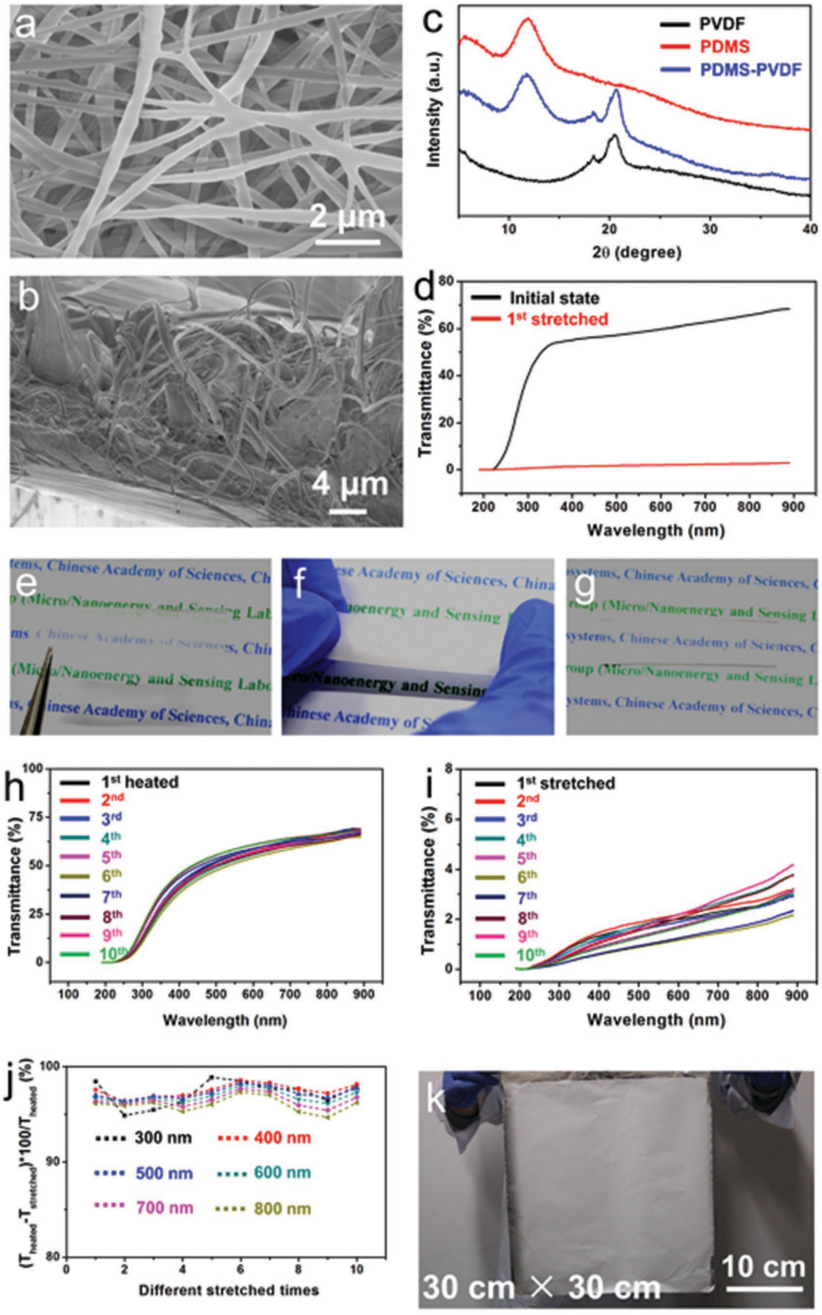

Figure 1. a) SEM image of PVDF nanowires. b) Cross-section SEM image of PVDF nanowires-PDMS composite film. c) XRD patterns of PVDF nanowires, PDMS, and the composite film. d) Transmittance of the composite film. e) Photograph of the composite film at the initial state. f) Photograph of the stretched composite film at the first time. g) Photograph of the composite film after the first heat treatment. h,i) Transmittance of the composite film after h) the heat treatment and i) the stretched treatment. j) Transmittance change ratio of the composite film. k) Photograph of the large-scale PVDF nanowires.

was measured under different heated and stretched times, as illustrated in Figure 1h,i, respectively. The stretched composite film exhibits a good repeatability to recover the transparent state after the heat treatment. The stretched composite film has a low transmittance with a ratio of below 5%. The change ratio δ of transmittance can be given by Equation (1):

$$\delta = \frac{T_{\text{heated}} - T_{\text{stretched}}}{T_{\text{heated}}} \quad (1)$$

where T_{heated} is the transmittance of the stretched composite film after the heat treatment and $T_{\text{stretched}}$ is the transmittance of the stretched composite film. As depicted in Figure 1j, the change ratio of transmittance exceeds 95% at all the different measurement times. Moreover, the PVDF nanowires can be grown on a large scale, as illustrated in Figure 1k. The modulation of the transmittance by applying stretched strains and heated temperatures has potential applications in smart windows and safety monitoring.

Usually, the transmittance of a film is an indicator of the miscibility of polymer blends.[24] The obtained PVDF nanowires have a high porosity and the small dimensions. The blend of PVDF nanowires and PDMS has a high transmittance at room temperature, indicating that the PVDF nanowires have a good miscibility with the PDMS.[24] Stretching will induce the separation between the matrix and the dispersed phase. Due to the difference in the anisotropic refractive indices between the matrix and the dispersed phase,[25] the transmittance of the composite film will be decreased under the stretched condition. When the stretched composite film was heated at 250 °C, the separation between the matrix and the dispersed phase can be decreased due to the melting of PVDF nanowires to achieve a good miscibility with PDMS. Thus, the light transmittance of the composite film can be dramatically increased under the heated temperature of 250 °C.

Figure 2a illustrates a schematic diagram of the hybridized nanogenerator including a PVDF nanowires–PDMS composite film and a poled PVDF film with the ITO electrodes on both surfaces. The hybridized nanogenerator integrates the TENG–PiENG and the PyENG into one device and same output electrodes. The flexible and transparent characteristics of the device can be clearly observed in Figure 2b,c, respectively.

The hybridized nanogenerator was fixed in an acrylic tube, where a flexible Nylon film was used as an oscillating membrane to produce the periodic contact and separation between the Nylon film and the PVDF nanowires–PDMS composite film. Figure 2d–f displays the working mechanism of the hybridized nanogenerator. Under a compressed/stretched stain on the poled PVDF film, the piezoelectric nanogenerator can produce output current/voltage signals due to the change in polarization intensity, as depicted in Figure 2d.

Adv. Mater. 2016,
DOI: 10.1002/adma.201505684

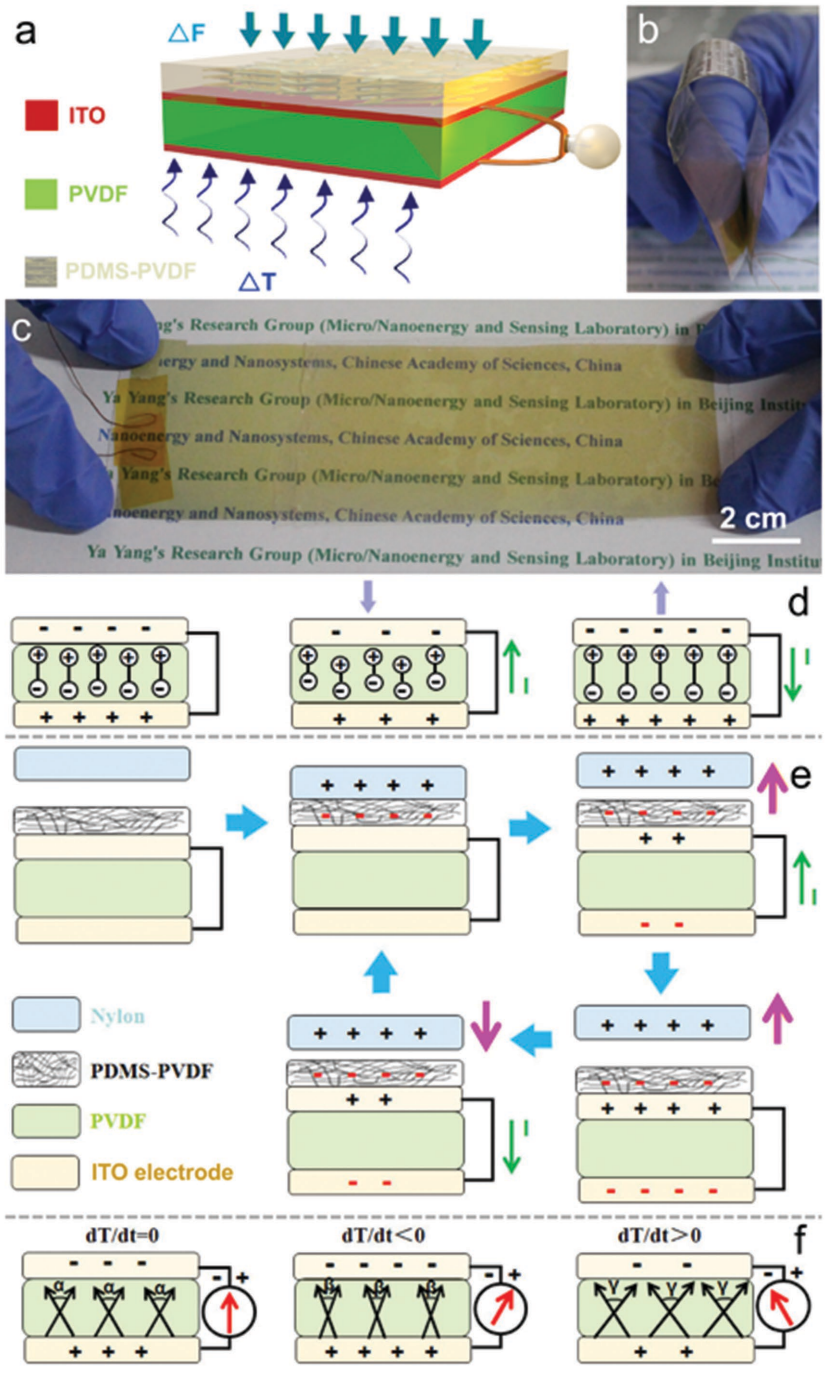

Figure 2. a) Schematic diagram of the hybridized nanogenerator. b) Photograph of the flexible hybridized nanogenerator. c) Photograph of the polarized PVDF film with the ITO electrodes on both surfaces. d–f) The working mechanisms of the PiENG (d), the TENG (e), and the PyENG (f). The magnitude of angle beta is smaller than that of the α, and the magnitude of angle γ is larger than that of the α.

For the TENG in Figure 2e, the electrons on the nylon film will be transferred to the surface of PVDF nanowires–PDMS composite film due to the different triboelectric polarities. When the separation between the Nylon film and the composite film appears, the triboelectric charges on the composite film will induce the flow of electrons from the top ITO electrode to the bottom ITO electrode due to electrostatic induction effect, which can result in the observed output current/voltages. The dynamic process for the flow of electrons is determined by both the triboelectric charges and the electrostatic induction. As displayed in Figure 2f, the mechanism of the PyENG is based on the thermally induced random wobbling of the electric dipole around its equilibrium axis.[20,21] When the poled PVDF film is cooled down, the spontaneous polarization will be enhanced since the electric dipoles oscillate within a smaller degree of spread angles due to lower thermal activity.[26] Due to electrostatic induction, the change in the spontaneous polarization can drive electrons to flow between the two ITO electrodes. When the temperature applied onto the poled PVDF film recovers to room temperature, the electric dipoles oscillate within a larger degree of spread around their respective alignment axes than that in cooled state; thus, the spontaneous polarization can be decreased, resulting in a flow of electrons in a reverse direction.

Figure 3a depicts the measured output current and output voltage signals of the TENG–PiENG under an air flow speed of about 15 m s^{-1}, indicating that the output current is about 20 μA and the output voltage is about 0.6 V under a loading resistance of 400 kOhm. To identify the respective contributions of TENG and PiENG to the obtained current/voltage signals, a controlled experiment of using a PET film to replace the poled PVDF film for a TENG has been achieved so that there is no PiENG in the device. As displayed in Figure S1a,b (Supporting Information), the TENG can deliver an output current of about 1.5 μA and output voltage of 0.4 V under a loading resistance of 400 kOhm. As compared with the output current and voltage signals in Figure 3a, it can be seen that the TENG has a much larger contribution to the output voltage than that of the PiENG, while the PiENG has a much larger contribution to the output current than that of the TENG.

When an external loading resistance was connected with the nanogenerator, the output current dropped with increasing loading resistance, while the output voltage increased with increasing loading resistance. The corresponding output power of TENG-PiENG increases in the resistance region from 1 to 20 kOhm and then decreases under a larger loading resistance (from 20 to 400 kOhm), where the output power was calculated by I^2R, where I is the output current and R is the loading resistance, as depicted

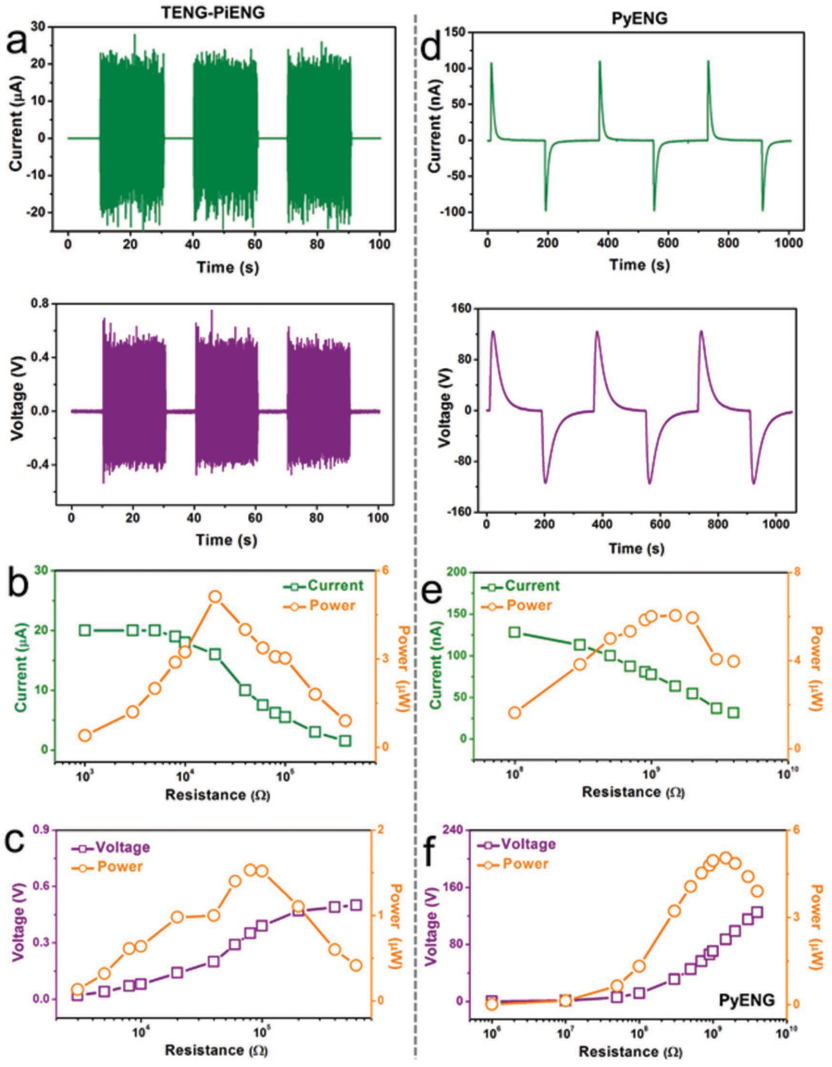

Figure 3. a,d) Measured output current and voltage signals of the TENG–PiENG (a) and the PyENG (d). b,e) Measured output current and the corresponding output powers of the TENG–PiENG (b) and the PyENG (e) under the different loading resistances. c,f) Measured output voltage and the corresponding output powers of the TENG–PiENG (c) and the PyENG (f) under the different loading resistances.

in Figure 3b. The largest output power of TENG–PiENG is about 5.12 μW under a loading resistance of 20 kOhm. The output power of the TENG–PiENG could also be calculated by U^2/R, where U is the output voltage and R is the loading resistance, as displayed in Figure 3c. The largest output power of the TENG–PiENG reaches 1.53 μW under a loading resistance of 80 kOhm. The large difference of impedance between the two calculation methods is associated with the TENG having a high impedance (Figure S1c,d, Supporting Information) while the PiENG has a low impedance. These results are consistent with the different contributions of the TENG and PiENG to the output voltage and current signals. Figure 3d presents the output current and voltage of PyENG under a temperature change of about −11 °C (Figure S2, Supporting Information), indicating that the output current and voltage peaks are about 120 nA and 120 V, respectively. As illustrated in Figure 3e, the largest output power of PyENG is about 6.05 μW under a loading resistance of 1.5 GOhm, which was calculated by using I^2R. By calculating the voltage data, the largest output power of PyENG is about 5.04 μW at a loading resistance of 1.5 GOhm, as displayed in Figure 3f. Although the output powers of the PyENG are slight different due to the different calculated methods, the same impedance values of 1.5 GOhm can be confirmed by analysis of the measured current and voltage data.

To understand the relationship between the TENG–PiENG/PyENG and the hybridized nanogenerator, the output current signals of the TENG–PiENG, PyENG, and the hybridized NG when both the TENG–PiENG and PyENG are working, are depicted in **Figure 4**a. Figure 4b displays an enlarged current signal of the PyENG under the temperature change of about −11 °C. By comparing the obtained current data, the hybridized nanogenerator has the same output current signals with that of the TENG–PiENG. The temperature-change-driven PyENG nearly has no contribution to the measured output current when both the TENG–PiENG and PyENG are working. Figure 4c illustrates the output voltages of the TENG–PiENG, PyENG, and the hybridized NG when both the TENG–PiENG and PyENG are working under a loading resistance of 4 GOhm. As depicted in Figure 4d, the output voltage of the TENG–PiENG is about 5 V, which is much smaller than that of the PyENG. The output voltage of the hybridized nanogenerator when both the TENG–PiENG and the PyENG are working is slightly smaller than that of PyENG.

As illustrated in Figure 4d, the output voltage of the TENG–PiENG is negative under positive connection to the measurement system, where the shape of the produced voltage signal is very similar to that of the PyENG. However, the PyENG has a positive output signal under the positive connection to the measurement system when a cooling temperature was applied to it (Figure 4c). The TENG–PiENG has a small negative output when the PyENG has a large positive output. Thus the hybridized nanogenerator has a smaller output voltage than that of the PyENG. A possible reason to explain the observed output voltage signals in Figure 4d is that the vibration of the Nylon film induced heat in the device when the TENG was working. To confirm that the heating temperature applied to the hybridized nanogenerator can result in negative output voltage signals under a positive connection to the measurement system, a controlled experiment was conducted, where the negative output voltage signals can be clearly observed when a heating temperature was applied on the device, as shown in Figure S3 (Supporting Information). The

Adv. Mater. **2016**,
DOI: 10.1002/adma.201505684

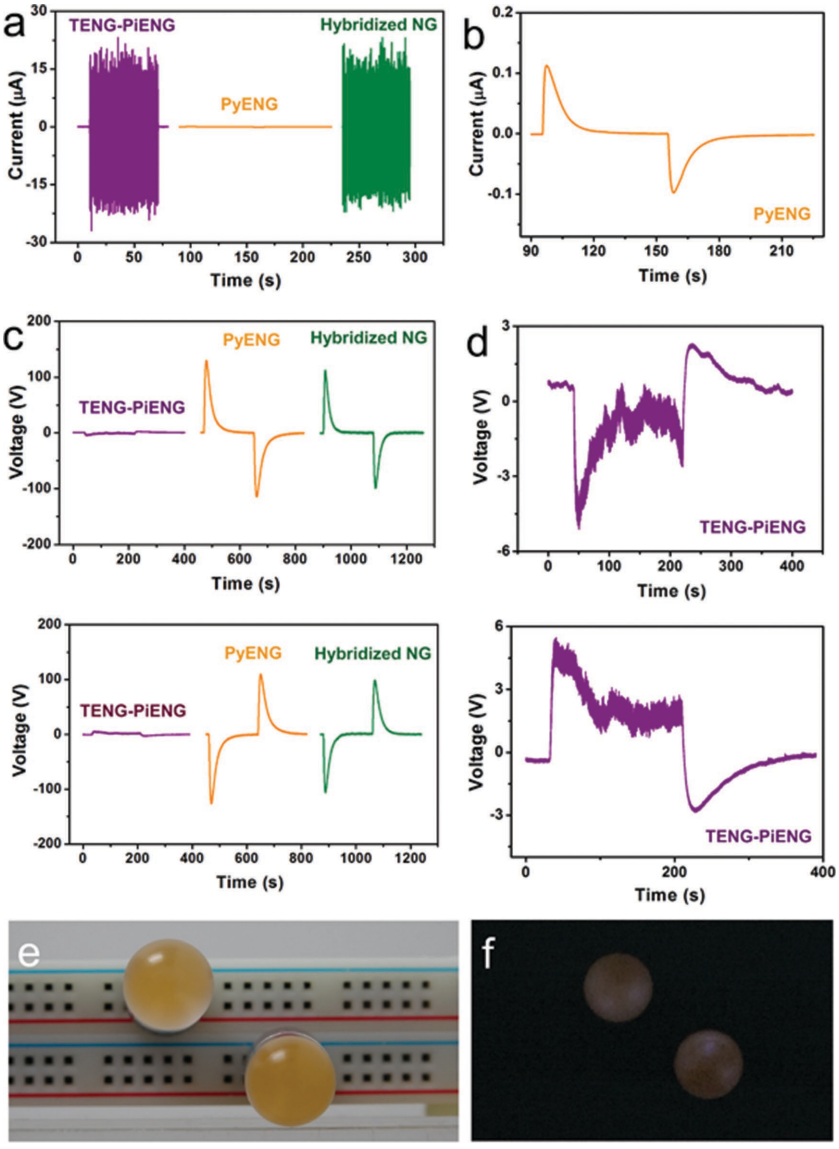

Figure 4. a) Measured output current signals of the TENG–PiENG, the PyENG, and the hybridized NG. b) Enlarged current signal of PyENG in (a). c) Measured output voltage signals of the TENG–PiENG, the PyENG, and the hybridized NG under the positive and reversed connection conditions. d) Enlarged voltage signals of TENG–PiENG. e) Photographs of two spot lights connected in series. f) Photograph of the two spot lights that can be lighted up by the hybridized NG.

obtained output voltages in Figure 4d is due to the coupling of the TENG–PiENG and the PyENG.

To demonstrate the application of the hybridized nanogenerator as a power source, two light bulbs were connected to the device, as illustrated in Figure 4e. The individual TENG–PiENG or PyENG cannot light up the two light bulbs in series due to the low voltage for the TENG–PiENG and the low current for the PyENG, while the light bulbs can be lit up when both the TENG–PiENG and PyENG are working, as displayed in Figure 4f and Movie S2 (Supporting Information). **Figure 5**a–f presents the measured rectified output current signals of the PyENG by a full-wave bridge circuit under working frequencies of 0.0083, 0.01, 0.0125, 0.0167, 0.025, and 0.05 Hz, respectively. Figure 5g shows the corresponding charging curves of a 10 μF capacitor under the different working frequencies of the PyENG. It can be found that the time interval between the beginning charging and the end of platform is consistent with the working frequency of the PyENG. The reason of step-like charging behavior is due to the low working frequencies of the PyENG. Figure 5h presents the different charging performances of the TENG–PiENG, PyENG (at the working frequency of 0.05 Hz), and the hybridized nanogenerator for the 10 μF capacitor. When both the TENG–PiENG and PyENG are working, the hybridized nanogenerator has a much better charging performance than that of the individual TENG–PiENG or PyENG.

In summary, we have demonstrated a hybridized nanogenerator with one device structure but contains different energy harvesting functions by using the piezoelectric, triboelectric, and pyroelectric effects. The hybridized nanogenerator with the structure of the PVDF nanowires–PDMS composite film/ITO electrode/poled PVDF film/ITO electrode consists of a TENG–PiENG and a PyENG for individually/simultaneously scavenging mechanical and thermal energies, respectively. As compared with the TENG–PiENG, the PyENG has a much larger output voltage but a smaller output current. When both the TENG–PiENG and the PyENG are working, the hybridized nanogenerator has a much better charging performance than that of the individual energy harvesting unit (TENG–PiENG or PyENG). This work will push forward a significant step toward hybridized energy harvesting in these places where the wind and temperature change simultaneously exist such as near active volcanos, geothermal sources, or at the top of hills.

Experimental Section

Fabrication of the Hybridized Nanogenerator: The nanogenerator consisted of a polarized PVDF film with a thickness of 120 μm and a PVDF nanowires–PDMS composite film. An ITO film with a thickness of 200 nm was sputtered onto the polarized PVDF film as electrode. Four acrylic sheets were cut by a laser cutting machine to fabricate an acrylic tube, where the height of the tube was 12 mm. A nylon film was fixed on the bluff body with the dimensions of 46 mm × 5 mm × 2 mm at the end of the acrylic tube. The polarized PVDF film with the ITO electrodes on the both sides was fixed on the inner surface of the acrylic tube. The PVDF nanowires–PDMS composite film was attached on the surface of the ITO/PVDF film/ITO. The vibration of the Nylon film can be driven by the wind in the acrylic tube, resulting in the

ADVANCED MATERIALS
www.advmat.de

www.MaterialsViews.com

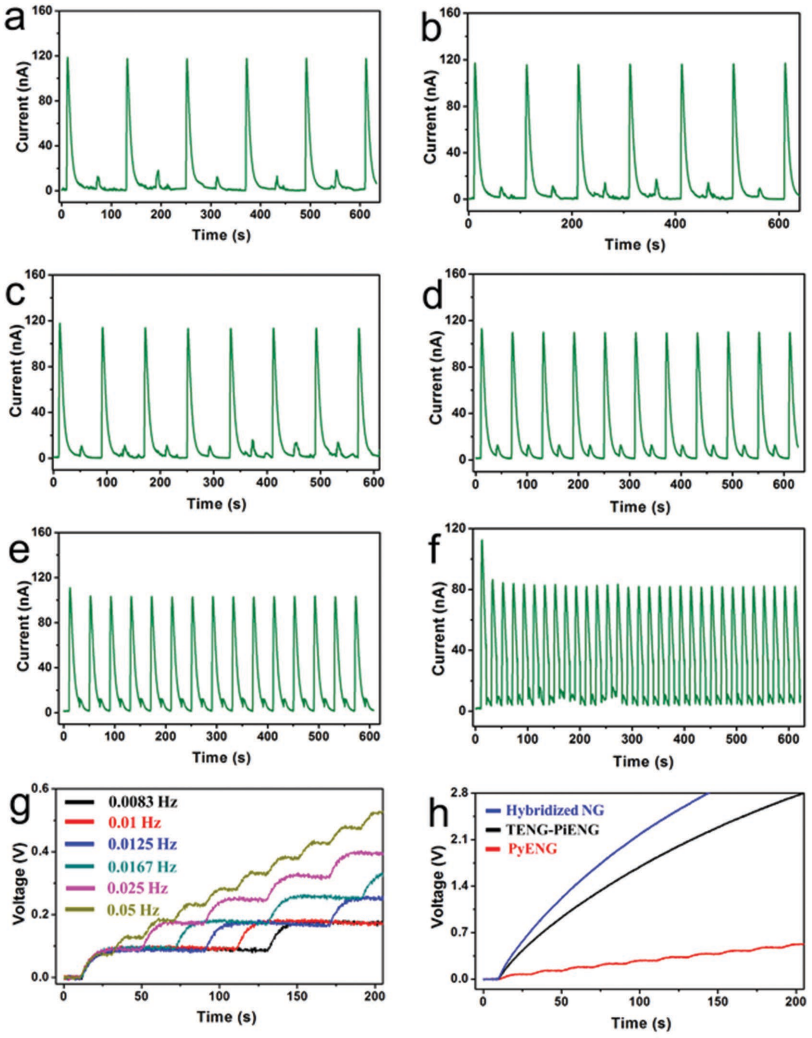

Figure 5. a–f) Measured rectified output current of the PyENG under different changing frequencies of 0.0083, 0.01, 0.0125, 0.0167, 0.025, and 0.05 Hz by using a rectifier, respectively. g) The charging curves of a 10 μF capacitor by using the PyENG under the different working frequencies. h) The measured voltage of the 10 μF capacitor charged by PyENG, TENG–PiENG, and the hybridized nanogenerator where both the PyENG and the TENG–PiENG are working.

periodic contact/separation between the nylon film and the polarized PVDF film. Thus, the TENG–PiENG can deliver the corresponding output voltage/current signals. Moreover, the output voltage/current signals of PyENG can be observed when the changing temperature was applied on the device.

Fabrication of the PVDF Nanowires-PDMS Composite Film: The PVDF nanowires–PDMS composite film was fabricated by using the following steps. First, the PVDF nanowires were fabricated by using an electrospinning method from 18 wt% polymer solution with a 1.83:1 weight ratio of *N*,*N*-dimethylformamide (DMF) to acetone.[27] The solution was stirring at 60 °C until the PVDF powder fully dissolved in the mixture solution, then was continuously stirred at room temperature for 12 h to obtain a homogeneous solution. The homogeneous solution was delivered into a 2.5 mL plastic syringe tipped with a 26-gauge stainless-steel needle at a rate of 0.5 mL h^{-1} under 20 kV.[27] The distance to the counter electrode was approximately 70 mm. A silicone elastomer and the crosslinker (Sylgard 184, Dow Corning) mixed in a 10:1 mass ratio was used to produce the mixture of PDMS solution. The PDMS monomer was mixed with its curing agent thoroughly, and then was subjected to vacuum to remove the trapped air. The PDMS mixture was then spin-coated (2000 rpm) onto the PVDF nanowires for 20 s. The PVDF nanowires–PDMS composite film was then placed in an oven at 80 °C for 3 h. After that, the fully dried transparent film was peeled away from the substrate, then was put onto the poled PVDF film.

Measurement of the Fabricated Hybridized Nanogenerator: The output current signals of the device were measured by a low-noise current preamplifier (Stanford Research SR570). The output voltage signals of the device were obtained by using a programmable electrometer (Keithley Model 6514). Transmittance of the PVDF nanowires–PDMS composite film was measured by a UV–vis spectrophotometer (Ultra-6600A) at different wavelengths. The crystal structure of PVDF nanowires–PDMS composite film was investigated from the wide-angle X-ray diffraction patterns taken on a X-ray diffractometer (X'Pert Pro). The morphology of the PVDF nanowires–PDMS composite film was examined using a field-emission scanning electron microscope (SU8020).

Supporting Information

Supporting Information is available from the Wiley Online Library or from the author.

Acknowledgements

This work was supported by Beijing Natural Science Foundation (Grant No. 2154059), National Natural Science Foundation of China (Grant Nos. 51472055 and 61404034), External Cooperation Program of BIC, Chinese Academy of Sciences (Grant No. 121411KYS820150028), and the "Thousands Talents" program for pioneer researcher and his innovation team, China. The authors would like to thank Zuqing Yuan for drawing schematic diagram of the hybridized nanogenerator.

Received: November 17, 2015
Revised: December 21, 2015
Published online:

[1] X. Wang, X. Lu, B. Liu, D. Chen, Y. Tong, G. Shen, *Adv. Mater.* **2014**, *26*, 4763.
[2] W. Zeng, L. Shu, Q. Li, S. Chen, F. Wang, X. M. Tao, *Adv. Mater.* **2014**, *26*, 5310.
[3] C. Zhang, H. Song, C. Liu, Y. Liu, C. Zhang, X. Nan, G. Cao, *Adv. Funct. Mater.* **2015**, *25*, 3497.
[4] H. G. Yoo, M. Byun, C. K. Jeong, K. J. Lee, *Adv. Mater.* **2015**, *27*, 3982.
[5] F. Zhao, H. Cheng, Z. Zhang, L. Jiang, L. Qu, *Adv. Mater.* **2015**, *27*, 4351.
[6] C. Xu, X. Wang, Z. L. Wang, *J. Am. Chem. Soc.* **2009**, *131*, 5866.
[7] C. Xu, Z. L. Wang, *Adv. Mater.* **2011**, *23*, 873.
[8] K. Y. Lee, M. K. Gupta, S.-W. Kim, *Nano Energy* **2015**, *14*, 139.

[9] Y. Zi, L. Lin, J. Wang, S. Wang, J. Chen, X. Fan, P. K. Yang, F. Yi, Z. L. Wang, *Adv. Mater.* **2015**, *27*, 2340.
[10] G. C. Yoon, K.-S. Shin, M. K. Gupta, K. Y. Lee, J.-H. Lee, Z. L. Wang, S.-W. Kim, *Nano Energy* **2015**, *12*, 547.
[11] S.-B. Jeon, D. Kim, G.-W. Yoon, J.-B. Yoon, Y.-K. Choi, *Nano Energy* **2015**, *12*, 636.
[12] Y. Y. Choi, P. Sharma, C. Phatak, D. J. Gosztola, Y. Liu, J. Lee, B. Lee, J. Li, A. Gruverman, S. Ducharme, S. Hong, *Nano Lett.* **2015**, *9*, 1809.
[13] Y. Y. Choi, T. G. Yun, N. Qaiser, H. Paik, H. S. Roh, J. Hong, S. Hong, S. M. Han, K. No, *Sci. Rep.* **2015**, *5*, 10728.
[14] F. X. Qin, J. Tang, V. V. Popov, J. S. liu, H. X. Peng, C. Brosseau, *Phys. Lett.* **2014**, *104*, 012901.
[15] D. Kim, H. S. Roh, Y. Kim, K. No, S. Hong, *RSC. Adv.* **2015**, *5*, 10662.
[16] S. Kim, M. K. Gupta, K. Y. Lee, A. Sohn, T. Y. Kim, K. S. Shin, D. Kim, S. K. Kim, K. H. Lee, H. J. Shin, D. W. Kim, S. W. Kim, *Adv. Mater.* **2014**, *26*, 3918.
[17] S. Y. Chung, S. Kim, J. H. Lee, K. Kim, S. W. Kim, C. Y. Kang, S. J. Yoon, Y. S. Kim, *Adv. Mater.* **2012**, *24*, 6022.
[18] D. Choi, M. Y. Choi, W. M. Choi, H. J. Shin, H. K. Park, J. S. Seo, J. Park, S. M. Yoon, S. J. Chae, Y. H. Lee, S. W. Kim, J. Y. Choi, S. Y. Lee, J. M. Kim, *Adv. Mater.* **2010**, *22*, 2187.
[19] G. T. Hwang, H. Park, J. H. Lee, S. Oh, K. I. Park, M. Byun, H. Park, G. Ahn, C. K. Jeong, K. No, H. Kwon, S. G. Lee, B. Joung, K. J. Lee, *Adv. Mater.* **2014**, *26*, 4880.
[20] Y. Yang, S. Wang, Y. Zhang, Z. L. Wang, *Nano Lett.* **2012**, *12*, 6408.
[21] Y. Yang, W. Guo, K. C. Pradel, G. Zhu, Y. Zhou, Y. Zhang, Y. Hu, L. Lin, Z. L. Wang, *Nano Lett.* **2012**, *12*, 2833.
[22] E. S. Cozza, O. Monticelli, E. Marsano, P. Cebe, *Polym. Int.* **2013**, *62*, 41.
[23] S. M. Damaraju, S. Wu, M. Jaffe, T. L. Arinzeh, *Biomed. Mater.* **2013**, *8*, 045007.
[24] S. Tang, P. Zou, H. Xiong, H. Tang, *Carbohydr. Polym.* **2008**, *72*, 521.
[25] Y. Maruhashi, S. Iida, *Polym. Eng. Sci.* **2001**, *41*, 1987.
[26] Y. Yang, J. H. Jung, B. K. Yun, F. Zhang, K. C. Pradel, W. Guo, Z. L. Wang, *Adv. Mater.* **2012**, *24*, 5357.
[27] L. Persano, C. Dagdeviren, Y. Su, Y. Zhang, S. Girardo, D. Pisignano, Y. Huang, J. A. Rogers, *Nat. Commun.* **2013**, *4*, 8.